JOURNAL OF AIRCRAFT
Vol. 47, No. 3, May–June 2010

Aerodynamic Performance of the Three-Dimensional Lifting Supersonic Biplane

Masahito Yonezawa* and Shigeru Obayashi†
Tohoku University, Sendai 980-8577, Japan

DOI: 10.2514/1.46651

This paper investigates the aerodynamic performance of the three-dimensional lifting supersonic biplane and its sonic boom. Although the Busemann biplane is known to cancel the wave drag, it does not produce lift, either. A few decades later, the supersonic biplane airfoils with lift were reported. This paper extends their ideas to the three-dimensional biplane. The aerodynamic performance was revealed by using computational fluid dynamics. The possibility of sonic boom mitigation due to shock wave interaction was demonstrated.

Nomenclature

AR	=	aspect ratio, b^2/S
b	=	span length
C_D	=	total drag coefficient
C_d	=	two-dimensional drag coefficient
C_{df}	=	two-dimensional friction drag coefficient
C_{dl}	=	two-dimensional wave drag coefficient due to lift
C_{dv}	=	two-dimensional wave drag coefficient due to volume
C_L	=	total lift coefficient
C_l	=	two-dimensional lift coefficient
C_{Mp}	=	pitching-moment coefficient
C_p	=	pressure coefficient
c	=	chord length
c_{ref}	=	reference chord length
c_{root}	=	root chord length
c_{tip}	=	tip chord length
h	=	wing clearance
M_∞	=	freestream Mach number
n	=	arbitrary point
S	=	reference area, $b \times c_{\text{ref}}$
s	=	staggering length
$t_{//\text{FS}}$	=	wing thickness parallel to freestream
x	=	chord length coordinate
y	=	spanwise coordinate
z	=	height coordinate
α	=	angle of attack, deg
β_1	=	oblique shock wave angle from the leading edge of the lower wing, deg
β'_1	=	oblique shock wave angle from the leading edge of the lower wing projected on the cross section, deg
β_2	=	oblique shock wave angle from the leading edge of the upper wing, deg
β'_2	=	oblique shock wave angle from the leading edge of the lower wing projected on the cross section, deg
β_3	=	diffracted oblique shock wave angle from the leading edge of the lower wing, deg
β_4	=	diffracted oblique shock wave angle from the leading edge of the upper wing, deg
$\beta_{\perp\text{LE}}$	=	oblique shock wave angle in the cross section perpendicular to the leading edge, deg
λ	=	taper ratio, $c_{\text{tip}}/c_{\text{root}}$
Ω	=	sweepback angle at the leading edge, deg

Subscripts

lower	=	lower wing
upper	=	upper wing

I. Introduction

SONIC boom mitigation and drag reduction are vital for realizing the new supersonic transport. For this objective, a lot of theories and techniques have been studied. The supersonic biplane theory, which was first introduced by Busemann [1], is also one of those theories. The major characteristic of the supersonic biplane is to be able to reduce the shock wave due to volume by the shock wave interaction. In recent years, Kusunose et al. [2] focused attention on this characteristic to reduce the sonic boom and have studied about the concept. They suggested the variable-shape mechanism for the supersonic biplane, avoiding the unstart phenomenon [3], and the biplane configuration with improved aerodynamic characteristics by the inverse design method [4].

This paper considers the three-dimensional lifting supersonic biplane. This is because the original supersonic biplane was considered in two dimensions, and the ideal configuration of the supersonic biplane under a lift condition is different from the supersonic biplane designed under zero lift. In addition, only the three-dimensional lifting supersonic biplane can give a good estimation of sonic boom mitigation due to shock wave interaction. The ideal configuration of the lifting supersonic biplane was first proposed by Moeckel [5] in 1947, and Licher [6] also introduced similar lifting multiple-plane configurations in 1955. However, they investigated the aerodynamic characteristics of only the two-dimensional lifting supersonic biplane and there have been no investigations of the three-dimensional lifting supersonic biplane. Tan [7] reported the most serious problem of the three-dimensional supersonic biplane. In the case of the three-dimensional rectangular supersonic biplane as an extension of the two-dimensional supersonic biplane airfoil in the spanwise direction, the shock wave interaction is disturbed at the wing tip and the disturbance spreads around the wing tip in the Mach cone shape. This disturbance induces a large drag penalty. However, Kusunose et al. [2] pointed out that changing the planform of the three-dimensional supersonic biplane could reduce the drag penalty. The geometry-definition method for the three-dimensional supersonic biplane was introduced and the sweep and taper effects on the three-dimensional supersonic biplane under the zero-lift condition was discussed [8].

In this paper, the geometry-definition method is extended to the three-dimensional lifting supersonic biplane, and the effects of geometry on the aerodynamic performance of the three-dimensional lifting supersonic biplane will be discussed using computational fluid

Received 8 August 2009; accepted for publication 21 December 2009.

*Ph.D. Candidate, Institute of Fluid Science, 2-1-1 Katahira, Aoba-ku. Student Member AIAA.

†Professor, Institute of Fluid Science, 2-1-1 Katahira, Aoba-ku. Associate Fellow AIAA.

dynamics (CFD) simulation. First, two-dimensional lifting supersonic biplanes with different design lift conditions were calculated to encompass the aerodynamic characteristics at various angles of attack. Then the effects of the geometric parameters were investigated in the three-dimensional lifting supersonic biplane at design lift. From the results, a high-aerodynamic-performance configuration of the three-dimensional lifting supersonic biplane was proposed. Finally, the sonic booms of three-dimensional lifting supersonic biplanes with various geometric parameters were estimated to evaluate the effects of their shock wave reduction on sonic boom mitigation and to investigate the effects of geometric parameters on the sonic boom.

II. Aerodynamic Analysis

A. Flow Computation

In this research, a three-dimensional unstructured flow solver named TAS code (Tohoku University Aerodynamic Simulation code) was used to simulate flowfields around the three-dimensional lifting supersonic biplane. Three-dimensional compressible Euler/Navier–Stokes equations were solved by a finite volume cell-vertex scheme. The numerical fluxes were computed using an approximate Riemann solver of the Harten–Lax–van Leer–Einfeldt–Wada scheme [9]. Second-order spatial accuracy was realized by linear reconstruction of the primitive gas-dynamic variables with Venkatakrishnan's limiter. The lower/upper symmetric Gauss–Seidel implicit method for an unstructured mesh [10] was used for time integration. The turbulence model used was the Spalart–Allmaras model [11]. To reduce the computational time, only the flowfields around half of the wing were simulated, and crossflows at the wing-root section were not considered.

When evaluating the effects of geometric parameters in a three-dimensional lifting supersonic biplane, the angle of attack was set to 1.313 deg. This angle of attack was calculated using Eq. (1), which is based on the thin-airfoil theory [2], to become $C_l = 0.1$ at $M_\infty = 1.7$, and the reference area was defined as the wing area of one wing:

$$C_l = \frac{3}{2}\frac{4\alpha}{\sqrt{M_\infty - 1}} \tag{1}$$

In viscous computation, the aerodynamic characteristics were analyzed at $Re = 30 \times 10^6$.

B. Mesh Generation

Unstructured mesh was provided for the present solver by using the EdgeEditor [12,13] and TU TetraGrid [14]. The characteristic point in the present mesh generation for calculating the supersonic biplane was to place a sufficient number of mesh points between two wings to capture the shock wave interaction, as shown in Fig. 1. This mesh was combined with a prism mesh on the biplane surface to resolve the boundary layer using the Navier–Stokes solver, as shown in Fig. 2 [15].

C. Overview of the Sonic Boom Estimation Process

The waveform parameter method developed by Thomas [16] was employed to estimate the sonic boom. Evaluation of the sonic boom was carried out in a four-step process, as described below:

1) The flowfield around the supersonic biplane was calculated using Euler computation.

2) The near-field pressure signature below the wing root was extracted from the computational result.

3) The waveform parameter method [16] was used to calculate the propagation of the near-field pressure-wave signature to the ground through the standard atmosphere model.

4) The pressure-wave signature estimated on the ground was evaluated.

In this study, the CFD simulation was carried out using the Euler solver of TAS code, as mentioned previously. In the sonic boom calculation, the flowfield around the aircraft was solved to extract the pressure-wave signature at a certain position located away from the

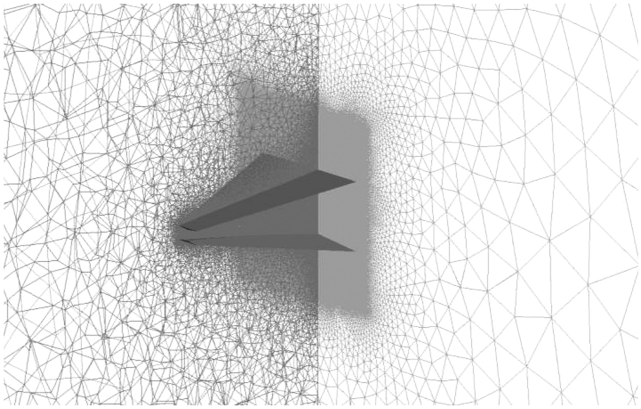

Fig. 1 Three-dimensional unstructured mesh.

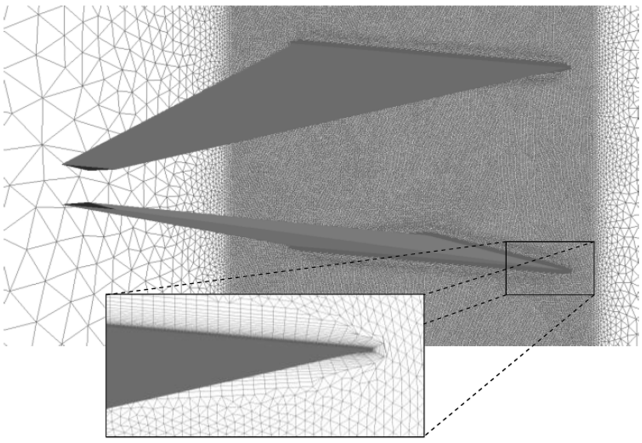

Fig. 2 Three-dimensional unstructured mesh with prismatic layer.

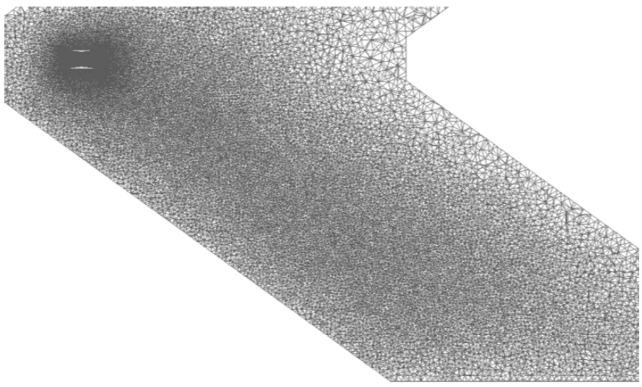

a) Previous mesh

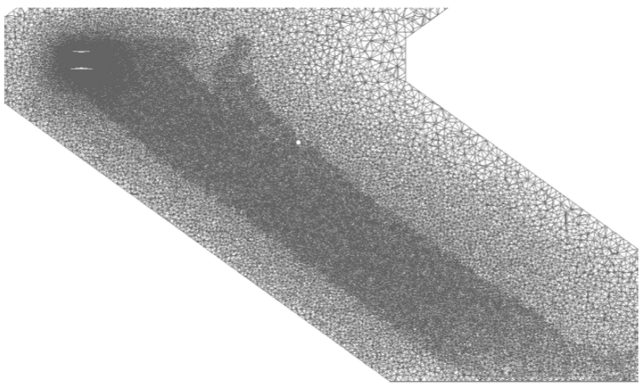

b) Refined mesh

Fig. 3 Computational meshes.

Table 1 Flight conditions for sonic boom calculation

Cruise Mach number	1.7
Cruise altitude	60,000 ft
Operating weight	7207 lb
Aircraft length (reference chord length)	7.530 ft
Ground reflection factor	1.9

fuselage. To obtain as accurate a solution as possible in a reasonable amount of time, the computational mesh must be refined up to where the near-field pressure signature is obtained. Therefore, the adaptive mesh refinement tool developed by Murayama et al. [17] was applied. The cells inside the high-pressure region near and under the biplane obtained from the calculation of the initial computational mesh were refined. Figure 3 shows the cutting plane of the initial and refined computational meshes at a spanwise location of 1 by reference chord length.

The flight conditions used in this analysis are shown in Table 1. The supersonic biplane was assumed to be undergoing a steady, straight, and level flight. The atmospheric conditions that were used in this analysis were the International Civil Aeronautics Organization 1976 standard atmosphere. In this analysis, the aircraft length was defined as the reference chord length. The reference area of the three-dimensional supersonic biplane was set to 4. For the sonic boom analysis, the operating weight was set to 7207 lb [16]. Thus, when the lift coefficient was assumed to be 0.10 and the aircraft length was assumed tobe the reference chord length of the three-dimensional supersonic biplane, its aircraft length became about 7.530 ft.

III. Geometry Definitions

A. Two-Dimensional Geometry

The geometry of the two-dimensional lifting supersonic biplane was defined as illustrated in Fig. 4. The shock wave diffraction was considered here. The vertex at the midchord was set at half of the chord length. The airfoil clearance, the staggering length, and the lower airfoil thickness (which are characteristic parameters of this lifting geometry designed at $M_\infty = 1.7$ and $t_{\text{upper}}/c = 0.05$) of the typical four C_l cases are shown in Table 2. The major difference in the geometric parameters from the zero-lift case is that the two airfoils are staggered based on the design lift condition (Table 2). The position of the leading edge of the lower airfoil is moved backward compared with that of the upper airfoil. The staggering length becomes larger when the wing has a higher angle of attack to generate more lift, although it is very small compared with the chord length, as shown in Table 2. With increasing angle of attack, the thickness of the lower airfoil becomes thicker to maintain the ideal shock wave interaction, and the clearance between the two airfoils also becomes wider.

B. Three-Dimensional Geometry

The geometry definition of the three-dimensional lifting supersonic biplane was defined as illustrated in Fig. 5. The definition process is described as follows:

1) A triangular airfoil was extended to a rectangular wing until a given aspect ratio, as shown in Fig. 5a.

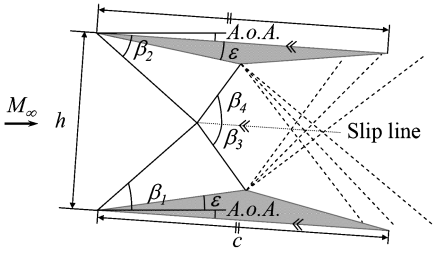

Fig. 4 Geometry of the two-dimensional lifting supersonic biplane (A.o.A. denotes angle of attack).

Table 2 Characteristic parameters of two-dimensional lifting supersonic biplane at $M_\infty = 1.7$ and $t_{\text{upper}}/c = 0.05$

	C_l			
	0.05	0.10	0.15	0.20
Name	Cl05	Cl10	Cl15	Cl20
α, deg [Eq. (1)]	0.656	1.313	1.969	2.626
h/c	0.516	0.528	0.541	0.554
s/c	0.00242	0.00495	0.00760	0.01043
t_{lower}/c	0.0558	0.0616	0.0674	0.0733

2) The trailing edge of the rectangular wing was tapered, as shown in Fig. 5b. The airfoil section was reduced in size gradually toward the tip, but the leading edge was kept perpendicular to the freestream. The vertex was always located at the midchord position on the cross section parallel to the freestream.

3) The tapered lower wing was swept back through a simple rotation around the root leading edge as shown in Fig. 5c. The wedge angle remained unchanged at all wing sections. Therefore, except inside the Mach cones at the wing root and tip, the shock front is always formed parallel to the leading edge and thus the shock wave interaction is not disturbed.

4) The upper wing with taper and sweepback was placed facing to the lower wing. As shown in Fig. 5d, the dihedral angle of the lower wing, anhedral angle of the upper wing, sweepback angle of the upper wing, and wing clearance were uniquely defined so that the oblique shock wave will hit the vertex of the other wing, by assuming

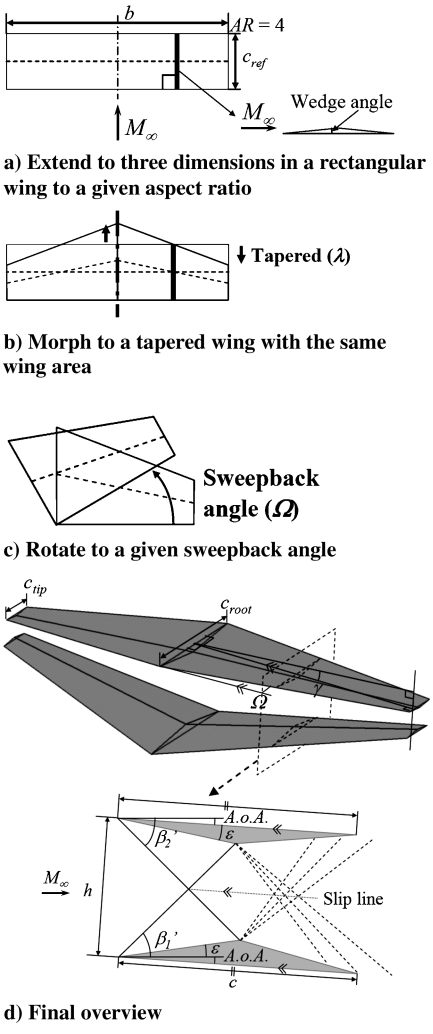

Fig. 5 Geometry definition of the three-dimensional lifting supersonic biplane.

Table 3 Given variables and dependent variables

Variables	Name	Value
Fixed	Reference area	4
Fixed	Aspect ratio	4
Fixed	Wedge angle, deg	5.71
Given	Taper ratio	0.1, 0.2, 0.3, 0.4
Given	Sweepback angle (lower wing), deg	10, 20, 30
Dependent	Sweepback angle (upper wing), deg	Determined from the taper ratio and sweepback angle
Dependent	Dihedral angle, deg	Determined from the taper ratio and sweepback angle
Dependent	Anhedral angle, deg	Determined from the taper ratio and sweepback angle
Dependent	Wing clearance	Determined from the taper ratio and sweepback angle
Dependent	Wing thickness	Determined from the taper ratio and sweepback angle

the linear shock wave theory without shock wave diffraction. The sweepback angle of the upper wing is defined automatically because the two wings are staggered. The oblique shock wave angle in the cross section perpendicular to the leading edge depends only on the sweepback angle and is unaffected by differences in taper ratio.

Table 3 shows the geometric parameters and values considered in this paper. In all configurations, the aspect ratio was fixed ($AR = b/c_{ref} = 4$). In addition, all the configurations had the same reference area ($S = b \times c_{ref} = 4$). The wedge angle of the upper wing was fixed at 5.71 deg, which corresponds to the wing thickness-to-chord ratio of 5%. Based on the wedge angle, the oblique shock wave angle from the leading edge can be calculated theoretically, which determines the wing clearance and dihedral angle. It has two independent variables, i.e., the taper ratio and the sweepback angle of the lower wing, and therefore 4 (taper ratio) by 3 (sweepback angle) different biplane configurations (12 total) were considered. Dihedral angle, anhedral angle, wing clearance, and wing thickness of the lower wing were uniquely and automatically determined from the other fixed and variable parameters. These conditions were defined to encompass the pure effect of the different sweepback angle and the taper ratio to the aerodynamic characteristics of the biplane and its geometry. In this section, the three-dimensional lifting supersonic biplane was designed to have equal $C_l = 0.10$. As an example of the present geometry definition, the geometry of the three-dimensional supersonic biplane with $\lambda = 0.2$ and $\Omega = 20$ deg is illustrated in Fig. 6.

IV. Aerodynamic Performance of the Two-Dimensional Lifting Supersonic Biplane

The aerodynamic characteristics of the original supersonic biplane ($C_l = 0.00$) and the lifting supersonic biplanes designed under four typical lift conditions ($C_l = 0.05$, 0.10, 0.15, and 0.20) were compared. Figure 7 shows the drag-polar curves of each configuration, and the outline symbols represent lift coefficients at the design conditions. The lift coefficient of each configuration at the corresponding design condition was nearly equal to its design lift coefficient. The drag-polar curvature became smaller when the design lift coefficient increased, as shown in Fig. 7. Figure 8 shows the comparison of the corresponding lift-to-drag ratios. Figure 8 indicates that the lift-to-drag ratio of the lifting supersonic biplane designed for $C_l = 0.05$ possesses the highest lift-to-drag ratio among the all configurations. In addition, the lift coefficient of each supersonic biplane at its maximum lift-to-drag ratio was different from the respective design lift coefficient. For example, $C_l = 0.09$ at the highest lift-to-drag ratio for the supersonic biplane designed at $C_l = 0.05$.

It was found that a lifting supersonic biplane gives its maximum lift-to-drag ratio at a different lift condition from the design lift condition. The lifting supersonic biplane designed at a slightly lower lift condition gives higher lift-to-drag ratio than the biplane designed at the given lift condition.

The lift-to-drag ratio at design lift condition was further examined. In Fig. 9, the lift-to-drag ratios evaluated by using CFD are plotted for eight different configurations. It has a maximum lift-to-drag ratio at $C_l = 0.10$. To explain the maximum, the design lift to the estimated drag was plotted in the black curve. The estimated drag coefficient is the sum of the uncanceled drag due to volume and the drag due to lift. The uncanceled drag due to volume was assumed to be 0.0021, which was based on the results for the supersonic biplane at zero lift analyzed by CFD simulation [2] and was plotted in the black dashed line. The drag due to lift was evaluated by Eq. (2) and plotted in a gray short dotted curve:

$$C_{dl} = \frac{3}{2}\frac{4\alpha^2}{\sqrt{M_\infty - 1}} \tag{2}$$

When these two drag components are equal, the maximum lift-to-drag is obtained. That is at about $C_l = 0.10$, where the black diamond-shaped point is plotted in Fig. 9.

If the viscous drag is considered, the maximum lift-to-drag ratio shifts to $C_l = 0.22$. The design lift to the estimated drag is given by the long dotted curve. The friction drag coefficient was assumed to be 0.0087, which was also based on the results of CFD simulation [2]. The sum of the friction drag and the uncanceled drag due to volume

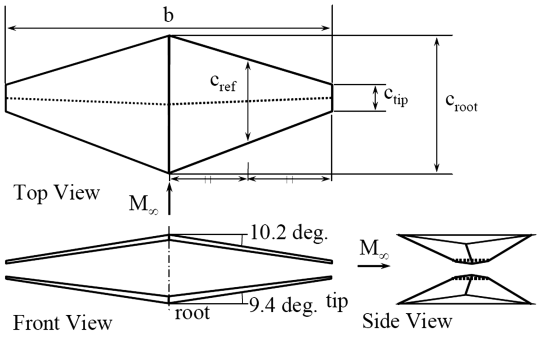

Fig. 6 Geometry of the three-dimensional lifting supersonic biplane ($\lambda = 0.2$ and $\Omega = 20$ deg).

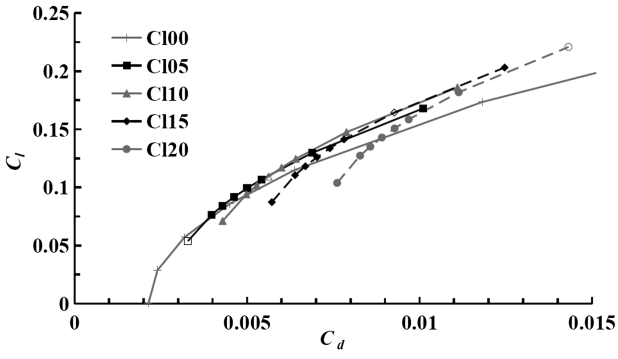

Fig. 7 Drag-polar curves of the lifting supersonic biplane.

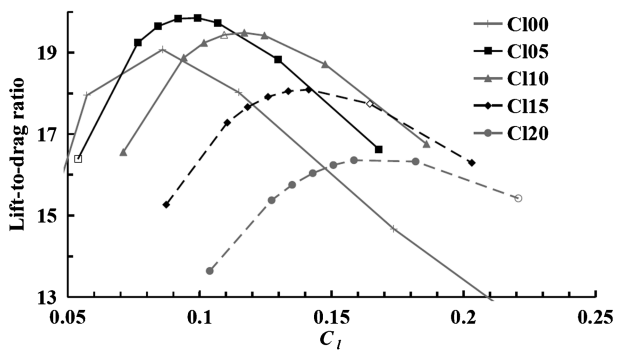

Fig. 8 Lift-to-drag ratio curves with lift coefficient.

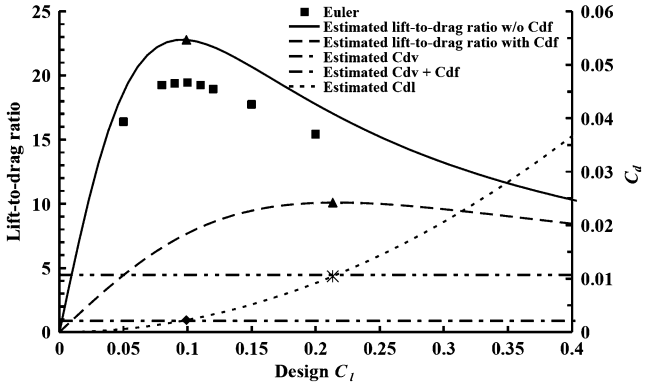

Fig. 9 Lift-to-drag ratio curves and drag coefficient of each drag components against theoretical lift coefficient.

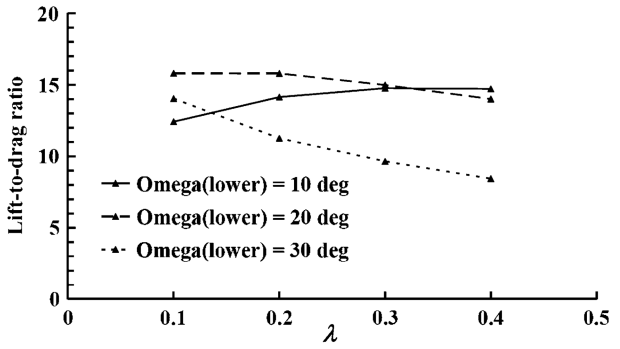

Fig. 11 Comparison of the lift-to-drag ratios for the three-dimensional lifting supersonic biplane designed under $C_l = 0.10$ with taper ratios and sweepback angles.

was plotted in the double-dashed line. Thus, estimated drag coefficient is the sum of the friction drag, the uncanceled drag due to volume, and the drag due to lift. At the asterisk point in Fig. 9, the sum of the friction drag and the uncanceled drag due to volume becomes equal to the drag due to lift.

The maximum lift-to-drag ratio was about 23 in the inviscid case and it was about 10 in the viscous case. Considering the friction drag, the lift condition that gives the maximum lift-to-drag ratio shifts from 0.1 to 0.2. The maximum lift-to-drag ratio is determined by the balance of drag components, pressure drag, and friction drag. On the other hand, the strength of the sonic boom will become smaller as the pressure drag is lower. Therefore, the supersonic biplane should be designed at the lift condition that gives the maximum lift-to-drag ratio to achieve the low drag and sonic boom.

V. Influences of Taper Ratio and Sweepback Angle in Three Dimensions

In this section, the effects of geometric parameters on the three-dimensional supersonic biplane are considered. All of the three-dimensional lifting supersonic biplanes designed under a design lift coefficient of 0.10, which is the same value as the average target lift coefficient of supersonic airplanes under a cruising condition, were calculated at $\alpha = 1.313$ deg. This angle of attack was calculated to be $C_l = 0.10$ by the thin-airfoil theory in a two-dimensional lifting supersonic biplane, as described previously. Comparisons of the lift coefficients and lift-to-drag ratios of the three-dimensional lifting supersonic biplanes with different taper ratios and sweepback angles are shown in Figs. 10 and 11, respectively.

As shown in Fig. 10, the lift coefficients of all the configurations examined were nearly equal to 0.10, which is the design lift coefficient used in this section. In more detail, in the case of $\Omega = 10$, 20, and 30 deg, the lift coefficient increased slightly, decreased slightly, and decreased markedly when the wing had a smaller taper ratio, respectively. As shown in Fig. 11, the configuration with $\Omega = 10$ deg had the highest lift-to-drag ratio of the configurations with $\lambda = 0.4$. Also, the configuration with $\Omega = 20$ deg had the highest lift-to-drag ratio of those examined, around $\lambda = 0.1$ and 0.2, and the configuration with $\Omega = 30$ deg had the highest lift-to-drag ratio of those examined, with $\lambda = 0.1$. In addition, the lift-to-drag ratio of the three-dimensional lifting supersonic biplane was the highest around the configuration with $\Omega = 20$ deg and $\lambda = 0.1$ and 0.2; the lift coefficient of the three-dimensional lifting supersonic biplane became about 0.103. Therefore, it was clarified that the geometry characteristics in the case of a high lift-to-drag ratio configuration of the three-dimensional lifting supersonic biplanes are similar to those in the case of the low-drag three-dimensional supersonic biplane under zero lift, as described in [8].

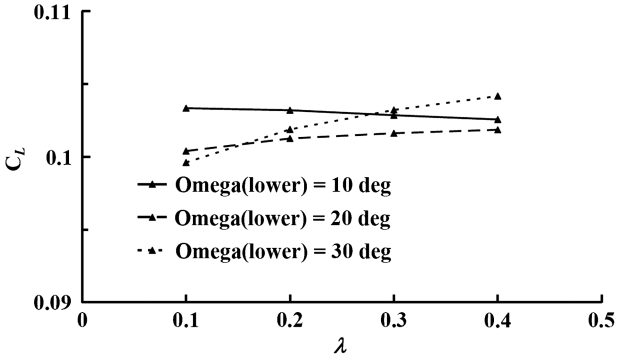

Fig. 10 Comparison of the lift coefficients for the three-dimensional lifting supersonic biplane designed under $C_l = 0.10$ with different taper ratios and sweepback angles.

VI. Aerodynamic Characteristics of the High-Aerodynamic-Performance Configuration

The geometric characteristics of the high-aerodynamic-performance configuration under the design lift of the three-dimensional lifting supersonic biplane were clarified as described in the previous section. In this section, the resulting three-dimensional lifting supersonic biplane (LSB) of $\Omega = 20$ deg and $\lambda = 0.2$, which is one of the high-aerodynamic-performance configurations under the design lift coefficient of 0.10, was calculated with changes in the angle of attack to evaluate its aerodynamic characteristics by viscous computation. In addition, its aerodynamic characteristics were compared with those of the rectangular supersonic biplane (RSB) with AR = 4 and those of the tapered supersonic biplane (TSB) with AR = 4 and $\lambda = 0.2$. Geometries of the RSB and TSB are illustrated in Figs. 12 and 13. Because RSB and TSB were evaluated in [18] using an Euler solver, their drag coefficient included a friction drag coefficient of 0.0087 [2]. The drag-polar curves of the RSB, TSB, and LSB are shown in Fig. 14, and the lift-to-drag ratio curves of the RSB, TSB, and LSB are shown in Fig. 15.

The drag-polar curvature of the LSB is smaller than those of the RSB and TSB because of the difference in the adopted airfoil. As indicated in [2], the curvature of the drag-polar curve of the two-dimensional lifting supersonic biplane is also smaller than that of the

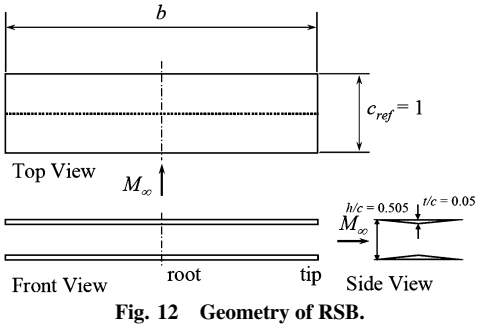

Fig. 12 Geometry of RSB.

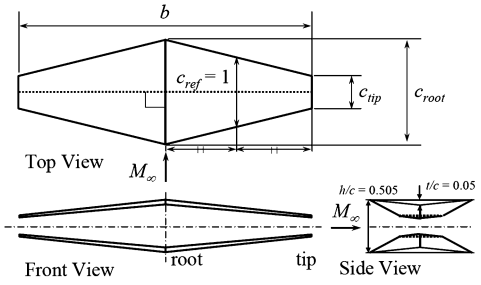

Fig. 13 Geometry of TSB.

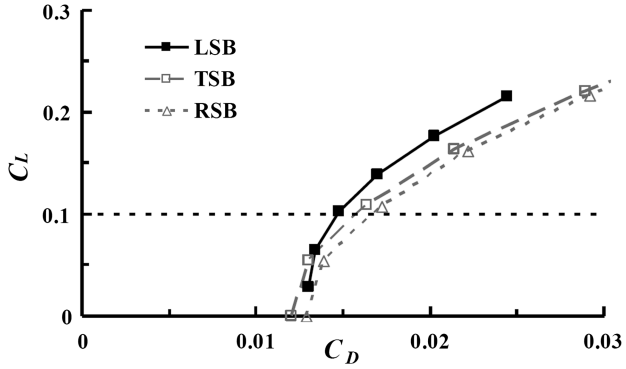

Fig. 14 Drag-polar curves of the RSB, TSB, and LSB.

two-dimensional supersonic biplane. This effect was reflected in the three-dimensional configuration. Comparing the drag coefficients at $C_L = 0.1$, the drag coefficient of the LSB is smaller by about 0.0020 than that of the RSB. Even the drag coefficient of the LSB is smaller by over 0.0010 than that of the TSB. In addition, the drag coefficient of the LSB was always smaller than those of the RSB and TSB at all lift coefficients above $C_L = 0.06$. As a result, the high-aerodynamic-performance configuration of the three-dimensional supersonic biplane also has high aerodynamic characteristics. As shown in Fig. 15, the difference between the lift-to-drag ratios of the RSB and TSB is small. However, the maximum lift-to-drag ratio of the LSB is around 8.8, which is an improvement of more than 1, compared with those of the RSB and TSB.

On the other hand, focusing on the static stabilities of these configurations, the aerodynamic centers can be calculated by Eq. (3):

$$\text{A.C.} = n + \frac{dC_{Mp}}{dC_1} \tag{3}$$

The pitching-moment coefficient was calculated as shown in Fig. 16, with the center of gravity defined as 0.5 c_{ref} on the x axis and defined from the leading edge of the wing root and the center location between two wings. In these cases, n was distance to the center of gravity from the leading edge of mean aerodynamic chord, which is

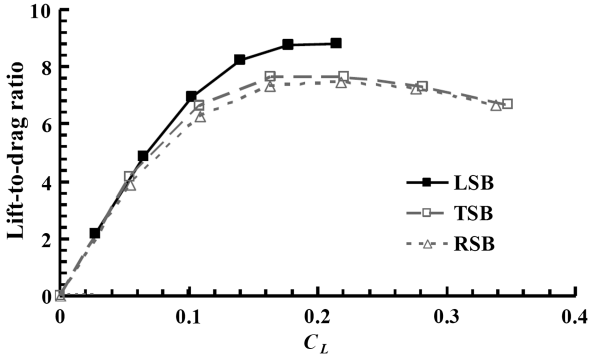

Fig. 15 Lift-to-drag ratio curves with lift coefficient of the RSB, TSB, and LSB.

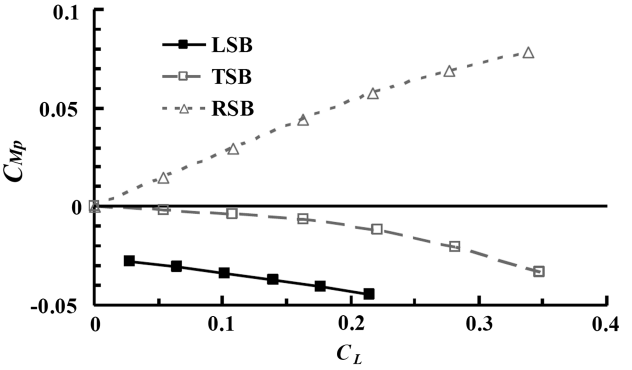

Fig. 16 Pitching-moment coefficient of the RSB, TSB, and LSB with the center of gravity defined as 0.5 c_{ref} on the x axis and defined from the leading edge of the wing root and the center location between two wings.

same as the reference chord in this paper, on the x axis. Thus, the aerodynamic center was calculated using Eq. (3). The aerodynamic center of the RSB was about 23%, that of the TSB was about 17%, and that of the LSB was 22%. The aerodynamic center of the TSB became closer to the leading edge. However, the aerodynamic center of the LSB is rarely different from that of the RSB. This result is responsible for the geometric effects. While the geometry characteristics of the TSB are that both edges are tapered and the vertex line at the midchord is perpendicular to the freestream, the vertex line of the LSB shows a slight sweepback. Thus, the aerodynamic center of the LSB is further back than that of TSB.

VII. Evaluation of the Sonic Boom

The possibility of sonic boom mitigation by the shock wave interaction in the three-dimensional lifting supersonic biplane was evaluated considering the geometry effects. The sonic booms of all of the above configurations of the three-dimensional lifting supersonic biplane with different taper ratios and sweepback angles were estimated and compared at $\alpha = 1.313$ deg.

A. Sonic Boom Mitigation by the High-Aerodynamic-Performance Configuration

This section evaluated the possibility of sonic boom mitigation by shock wave interaction using the three-dimensional lifting supersonic biplane with $\Omega = 20$ deg and $\lambda = 0.2$, which is one of the high-aerodynamic-performance configurations under the design lift coefficient of 0.10. A preliminary analysis was carried out to determine the position at which the near-field pressure-wave signature should be extracted for the input data to the wave parameter method. For this analysis, the refinement meshes indicated in Sec. II.C were used. The sonic booms on the ground were calculated

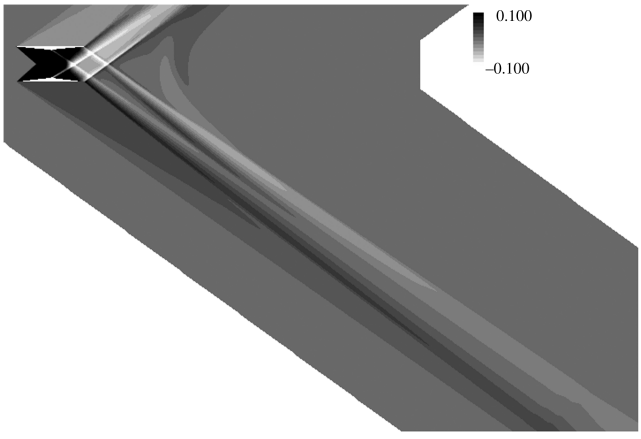

Fig. 17 C_p contour plot on the symmetry plane for the three-dimensional lifting supersonic biplane with $\Omega = 20$ deg and $\lambda = 0.2$.

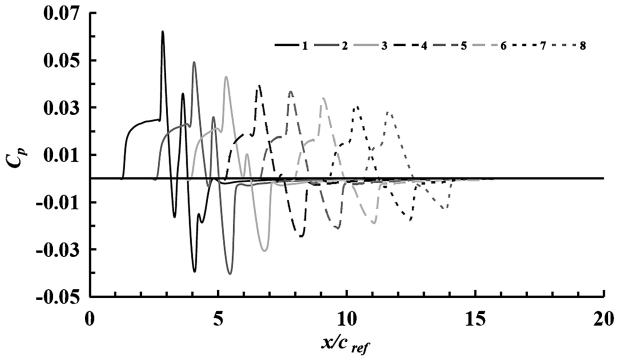

Fig. 18 Near-field C_p distributions for the three-dimensional lifting supersonic biplane with $\Omega = 20$ deg and $\lambda = 0.2$.

from these near-field pressure signatures using the wave parameter method. To evaluate the sonic boom accurately, the near-field pressure signature at the appropriate location had to be chosen.

The appropriate position to extract the near-field pressure-wave signature was selected by comparing the estimated sonic boom signature on the ground of the three-dimensional lifting supersonic biplane with $\Omega = 20$ deg and $\lambda = 0.2$. The C_p contour plot on the symmetry plane is shown in Fig. 17. The C_p distributions at $z/c_{\text{ref}} = 1, 2, 3, 4, 5, 6, 7$, and 8 below the wing were extracted at the symmetry plane and each sonic boom was estimated under the condition described in Table 1.

These near-field C_p distributions extracted from the symmetry plane are shown in Fig. 18, and the ground sonic boom signatures are shown in Fig. 19. The compression wave became a gentle initial rise. In addition, a few overspill pressure waves were generated behind the high-pressure wave. The peaks of the ground sonic boom signatures continued to increase when z/c_{ref} became 6, due to three-dimensionality. As a result, the appropriate altitude to extract the near-field pressure-wave signature was selected as $z/c_{\text{ref}} = 6$.

On the other hand, considering the sonic boom strength, the maximum peak of the sonic boom was about 0.4 psf and that of the negative peak was about 0.3 psf. From the target value of the sonic boom for new supersonic transport of 0.5 psf, these values of the three-dimensional lifting supersonic biplane with $\Omega = 20$ deg and $\lambda = 0.2$ demonstrate the potential of sonic boom mitigation due to the shock wave interaction. Although the three-dimensional supersonic biplane is not a full aircraft configuration yet, the supersonic biplane has a very strong possibility for sonic boom mitigation. When these results were calculated with an operating weight nearly equal to that of the Japan Aerospace Exploration Agency's flight demonstrator [19], whose target value of the maximum sonic boom is also 0.5 psf, the maximum sonic boom was kept below 0.5 psf.

B. Influences of the Geometric Parameters on the Sonic Boom

The effects of the geometric parameters on the sonic boom were next examined. The near-field C_p distributions of the above three-dimensional lifting supersonic biplane with different taper ratios and sweepback angles were extracted at $z/c_{\text{ref}} = 6$. The very small difference in the lift coefficients of 0.10 was ignored in each configuration, and thus the lift coefficient was assumed as 0.10. The near-field C_p distributions and ground sonic boom signatures are shown in Figs. 20 and 21, respectively.

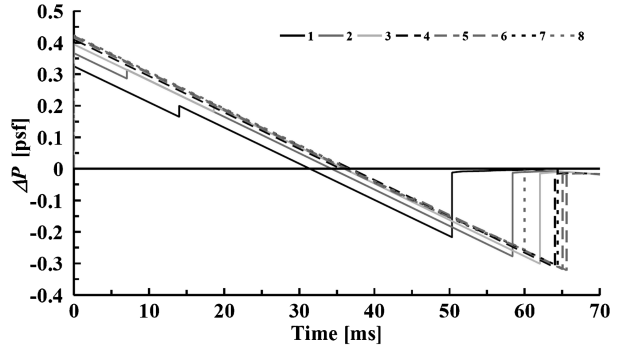

Fig. 19 Ground sonic boom signatures for the three-dimensional lifting supersonic biplane with $\Omega = 20$ deg and $\lambda = 0.2$.

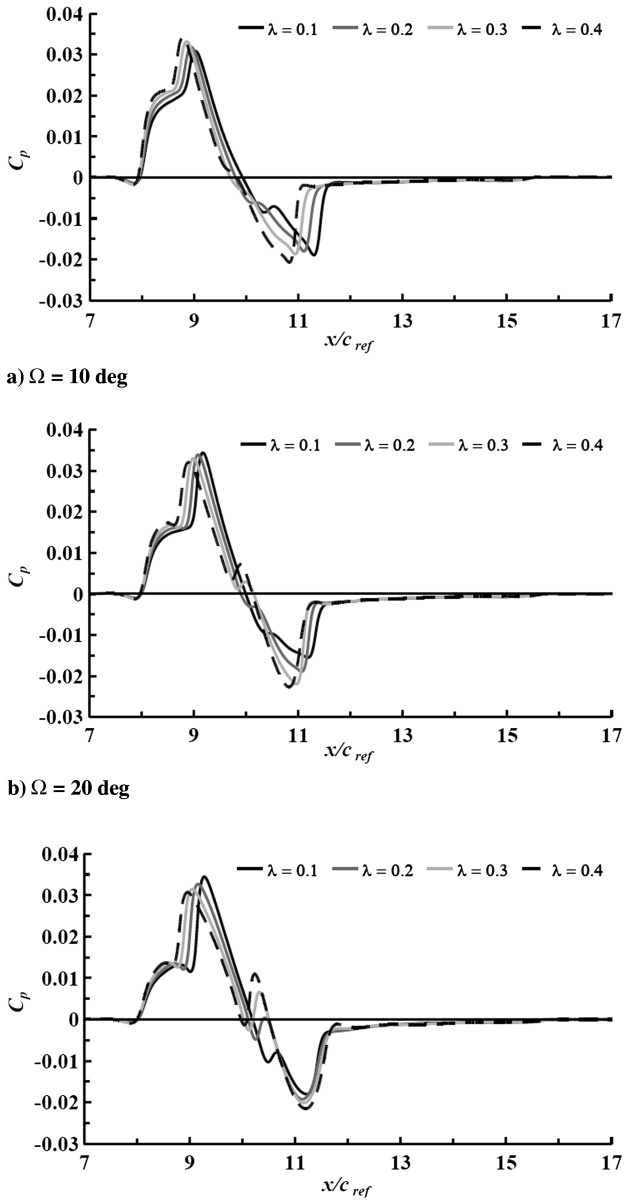

Fig. 20 Near-field C_p distributions for the three-dimensional lifting supersonic biplanes below the lower wing at a distance of six reference chord lengths.

As shown in Fig. 20, the initial rise of the C_p distribution became larger when the wing had a larger taper ratio at each sweepback angle. The initial rise also became larger as the sweepback angle increased. The high-pressure peak behind the initial rise approached the initial rise when the wing had a larger taper ratio. The secondary pressure peak, due to pressure recovery and overspill shock wave, was clear in the case of $\Omega = 30$ deg. In addition, the strength of this peak became weaker when the wing had a larger taper ratio. As shown in Fig. 21, the values of the maximum and minimum peaks of the sonic boom were almost the same for all configurations, although some differences were observed in the near-field C_p distributions. In the case of the $\Omega = 30$ deg, a few sonic booms had a second peak. Thus, the results indicated that the geometric parameters had no influence on the sonic boom.

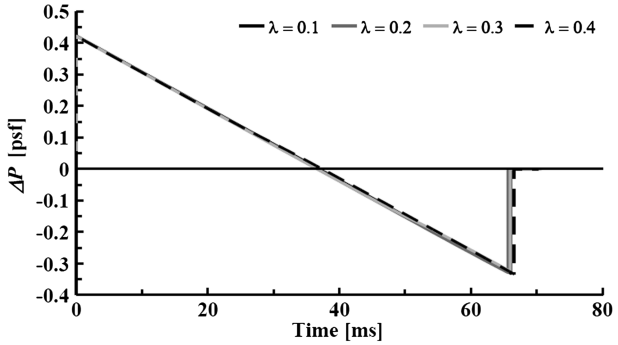

a) Ω = 10 deg

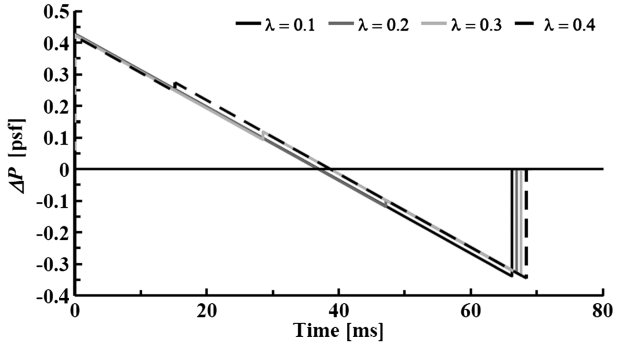

b) Ω = 20 deg

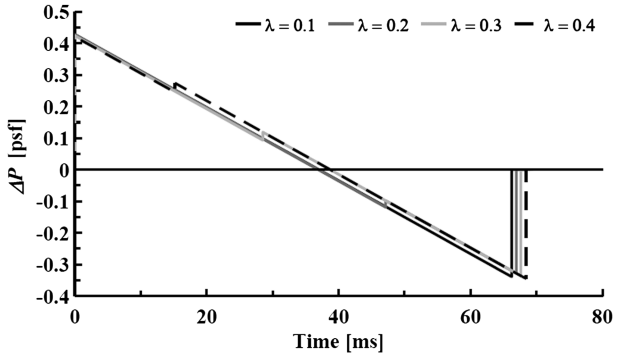

c) Ω = 30 deg

Fig. 21 Ground sonic boom signatures for the three-dimensional lifting supersonic biplane.

VIII. Conclusions

This paper presented analysis of the aerodynamic characteristics of the high-aerodynamic-performance configuration of the three-dimensional lifting supersonic biplane. The geometry-definition method was created to define the three-dimensional lifting supersonic biplane following Moeckel's [5] and Licher's [6] two-dimensional idea. In the present study, its aerodynamic characteristics were evaluated in detail by using the CFD.

Based on the previous studies [5,6], the two-dimensional lifting supersonic biplane was defined. The designed two-dimensional supersonic biplane achieved the design lift coefficient at the design angle of attack. It was found that the lifting supersonic biplane designed at a slightly lower lift gives a larger lift-to-drag ratio at the given lift condition. In addition, the lifting supersonic biplane designed can obtain the maximum lift-to-drag ratio at the design lift condition, as the wave drag due to lift was equal to the sum of the other drag components at the design lift condition.

The geometric parameters of the high-aerodynamic-performance configuration of the three-dimensional lifting supersonic biplane are similar to those of the low-drag configuration of the three-dimensional supersonic biplane. For example, the three-dimensional lifting supersonic biplane with $\Omega = 20$ deg and $\lambda = 0.2$ is one of the configurations with the best aerodynamic performance.

Next, the aerodynamic characteristics of the three-dimensional supersonic biplane with $\Omega = 20$ deg and $\lambda = 0.2$ were evaluated. The drag coefficient of the high-aerodynamic-performance configuration at the designed condition became smaller than that of the no-lifting designs. The maximum lift-to-drag ratio became 8.8 even though the biplane has two surfaces as the wet area.

Furthermore, the geometry effects for the sonic booms were evaluated. The values of the maximum and minimum peaks of the estimated sonic boom were under about 0.4 psf for all configurations investigated when the operating weight was set to 7207 lb. Thus, the three-dimensional lifting supersonic biplane showed the strong possibility of sonic boom mitigation by the shock wave interaction. Further study should be performed on an actual aircraft configuration and its sonic boom, because the fuselage, engine nacelle, etc., are required to realize an actual aircraft, and the shock wave, propagating to the ground, occurs from these parts.

References

[1] Busemann, A., "Aerodynamic Lift at Supersonic Speed," *Luftfahrtforschung*, Vol. 12, No. 6, 1935, pp. 210–220.

[2] Kusunose, K., Matsushima, K., Obayashi, S., Furukawa, T., Kuratani, N., Goto, Y., Maruyama, D., Yamashita, H., and Yonezawa, M., *Aerodynamic Design of Supersonic Biplane: Cutting Edge and Related Topics*, Tohoku Univ. Press, Sendai, 2007.

[3] Yamashita, H., Obayashi, S., and Kusunose, K., "Reduction of Drag Penalty by Means of Plain Flaps in the Boomless Busemann Biplane," *International Journal of Emerging Multidisciplinary Fluid Sciences*, Vol. 1, No. 2, June 2009, pp. 141–164. doi:10.1260/175683109788707490

[4] Maruyama, D., Matsushima, K., and Nakahashi, K., "Aerodynamic Analyses of Airfoil Configurations of Biplane Type Supersonic Transport," *Transactions of the Japan Society of Mechanical Engineers, Series B*, Vol. 72, No. 721, 2006, pp. 2132–2139 (in Japanese).

[5] Moeckel, W. E., "Theoretical Aerodynamic Coefficients of the Two-Dimensional Supersonic Biplane," NACA TN-1316, 1947.

[6] Licher, R. M., "Optimum Two-Dimensional Multiplanes in Supersonic Flow," Douglas Aircraft Co., Rept. SM-18688, Santa Monica, CA, 1955.

[7] Tan, H. S., "The Aerodynamics of Supersonic Biplanes of Finite Span," Wright Air Development Center, TR 52-276, Dayton, OH, 1950.

[8] Yonezawa, M., and Obayashi, S., "Reducing Drag Penalty in the Three-Dimensional Supersonic Biplane," *Proceedings of the Institution of Mechanical Engineers, Part G (Journal of Aerospace Engineering)*, Vol. 223, No. 7, 2009, pp. 891–899. doi:10.1243/09544100JAERO521. DOI:

[9] Obayashi, S., and Guruswamy, G. P., "Convergence Acceleration of a Navier-Stokes Solver for Efficient Static Aeroelastic Computations," *AIAA Journal*, Vol. 33, No. 6, 1995, pp. 1134–1141. doi:10.2514/3.12533

[10] Sharov, D., and Nakahashi, K., "Reordering of Hybrid Unstructured Grids for Lower-Upper Symmetric Gauss-Seidel Computations," *AIAA Journal*, Vol. 36, No. 3, 1998, pp. 484–486. doi:10.2514/2.392

[11] Spalart, P. R., and Allmaras, S. R., "A One-Equation Turbulence Model for Aerodynamics Flows," AIAA Paper 92-0439, 1992.

[12] Ito, Y., and Nakahashi, K., "Direct Surface Triangulation Using Stereolithography Data," *AIAA Journal*, Vol. 40, No. 3, March 2002, pp. 490–496. doi:10.2514/2.1672

[13] Ito, Y., and Nakahashi, K., "Surface Triangulation for Polygonal Models Based on CAD Data," *International Journal for Numerical Methods in Fluids*, Vol. 39, No. 1, May 2002, pp. 75–96. doi:10.1002/fld.281

[14] Sharov, D., and Nakahashi, K., "A Boundary Recovery Algorithm for Delaunay Tetrahedral Meshing," *Proceedings of the 5th International Conference on Numerical Grid Generation in Computational Field Simulations*, NSF Engineering Research Center for Computational Field Simulation, Mississippi State Univ., Mississippi State, MS, 1996, pp. 229–238.

[15] Ito, Y., and Nakahashi, K., "Improvements in the Reliability and Quality of Unstructured Hybrid Mesh Generation," *International Journal for*

Numerical Methods in Fluids, Vol. 45, No. 1, May 2004, pp. 79–108. doi:10.1002/fld.669

[16] Thomas, C. L., "Extrapolation of Sonic Boom Pressure Signatures by the Waveform Parameter Method," NASA, TN D-6832, 1972.

[17] Murayama, M., Nakahashi, K., and Sawada, K., "Simulation of Vortex Breakdown Using Adaptive Grid Refinement with Vortex-Center Identification," *AIAA Journal*, Vol. 39, No. 7, July 2001, pp. 1305–1312.
doi:10.2514/2.1448

[18] Yonezawa, M., and Obayashi, S., "CFD Analysis Based Evaluation of Aerodynamic Characteristics for Supersonic Biplane with Finite Span Length," *Journal of the Japan Society for Aeronautical and Space Sciences*, Vol. 57, No. 660, 2009, pp. 32–38 (in Japanese).

[19] Sato, K., Kumano, T., Yonezawa, M., Yamashita, H., Jeong, S., and Obayashi, S., . "Low-Boom and Low-Drag Optimization of the Twin Engine Version of Silent Supersonic Business Jet," *Journal of Fluid Science and Technology*, Vol. 3, No. 4, 2008, pp. 576–585.
doi:10.1299/jfst.3.576